Structural and magnetic properties of $La_{0.7}Pb_{0.3}(Mn_{1-x}Fe_x)O_3$ ($0 \leqslant x \leqslant 0.3$) giant magnetoresistance perovskites

J. Gutiérrez
Departamento de Electricidad y Electrónica, Universidad del País Vasco/EHU, Box 644, E-48080 Bilbao, Spain

A. Peña
Departamento de Química Inorgánica, Universidad del País Vasco/EHU, Box 644, E-48080 Bilbao, Spain

J. M. Barandiarán
Departamento de Electricidad y Electrónica, Universidad del País Vasco/EHU, Box 644, E-48080 Bilbao, Spain

J. L. Pizarro
Departamento Mineralogía y Petrología, Universidad del País Vasco/EHU, Box 644, E-48080 Bilbao, Spain

T. Hernández
Departamento de Electricidad y Electrónica, Universidad del País Vasco/EHU, Box 644, E-48080 Bilbao, Spain

L. Lezama, M. Insausti, and T. Rojo
Departamento de Química Inorgánica, Universidad del País Vasco/EHU, Box 644, E-48080 Bilbao, Spain
(Received 8 June 1999)

Neutron-diffraction, magnetic and transport measurements, and Mössbauer spectroscopy have been used in order to study the structural and magnetic changes of the magnetoresistive $La_{0.7}Pb_{0.3}Mn_{1-x}Fe_xO_3$ ($x=0$, 0.05, 0.1, 0.2, 0.3) perovskitelike compounds. Samples were prepared by the sol-gel low-temperature method. In all cases the exact stoichiometry is different from the nominal one probably due to the presence of cation vacancies. All the phases exhibit ferromagnetic behavior except the compositions with the highest Fe contents ($x=0.2$, 0.3), which show spin-glass order. A 10% Fe contribution lowers the T_C by about 130 K. The magnetic moment continuously decreases with the increasing amount of iron. The magnetoresistance [MR $=\Delta R/R(0)$], between 0 and 6 T applied fields, has been measured only in the $x=0.05$ and 0.1 compositions, being of about 65% around the magnetic transition in the case of the 10% Fe content sample. For higher Fe contents, the samples show clearly insulating trends. These results can be interpreted in terms of a hindering of the double-exchange mechanism by Fe^{3+} ions, which gives rise to the localization of the electronic carriers and to a subsequent frustration of the long-range magnetic order.

I. INTRODUCTION

The rare-earth manganites of the type $L_{1-x}A_xMnO_3$, where L is La^{3+}, Sm^{3+}, Pr^{3+}, Nd^{3+} and A is Ca^{2+}, Pb^{2+}, Sr^{2+}, Ba^{2+}, Cd^{2+}, have attracted the attention of the scientific community due to the colossal magnetoresistance, (CMR) phenomenon exhibited when the ferromagnetic ordering of Mn spins occurs.[1–3]

The magnetic and transport properties of these samples are determined by several factors such as the percentage of the divalent ions, the ionic radii of the metal ions, the method used in the preparation of the samples, etc.[4–6] These properties have traditionally been examined within the framework of the ''double-exchange'' theory which considers the magnetic coupling between Mn^{3+} and Mn^{4+} ions.[7] The amount of pairs of Mn^{3+} and Mn^{4+} changes due to the doping level of the perovskite or its oxygen stoichiometry. In both cases the result is a distortion of the perovskite structure that has direct influence not only on the Mn-O distance, but also on the angle of the Mn^{3+}-O-Mn^{4+} bond. It has also been observed that the ferromagnetic coupling and the metal-insulator transition temperature are very sensitive to the change of these parameters.

In a similar way, the substitution of the Mn ions by other transition metal ions in perovskites of composition $L_{0.7}A_{0.3}Mn_{1-y}T_y^{3+}O_3$ (T=transition metal), which shows ferromagnetism and CMR for the $y=0$ sample, gives rise also to changes in the Mn^{3+}:Mn^{4+} proportion. This alters the magnetic coupling between these ions, which is reflected in a gradual weakening of the ferromagnetism as the doping level of the T^{3+} ion increases, with important modifications in the magnetic and transport properties.[5–6,8]

Regarding the possible technical applications, good magnetotransport properties occurring at or close to ambient temperatures[9] are required. In this sense, Pb-doped perovskites exhibit critical temperatures close to 300 K,[10,11] offering so the possibility of realizing a technologically useful magnetoresistive effect magnitude around room temperature.

In this work we report structural, magnetic, and magnetoresistive properties of $La_{0.7}Pb_{0.3}(Mn_{1-x}Fe_x)O_3$ ($x=0$, 0.05, 0.1, 0.2, 0.3) which have been prepared by the sol-gel low-temperature method.[12] This method presents the advantage

of using low-temperature synthesis, which results not only in smaller grains, but also produces high-purity and homogeneous powders which are easy to use in order to prepare samples. We have focused our effort on the study of the effect caused by the substitution of a substantially big amount of Mn by Fe ions, up to a 30%, in the samples. We have translated the changes in all those properties to fundamental electronic competitions between Mn^{3+}-Mn^{4+} and Fe^{3+}-Mn^{4+} pairs.

II. EXPERIMENT

Mixed oxides of $La_{0.7}Pb_{0.3}(Mn_{1-x}Fe_x)O_3$, $x=0$, 0.05, 0.1, 0.2, 0.3, compositions were prepared by the sol-gel method with the required quantities of La_2O_3, $Pb(NO_3)_2$, $Mn(C_2H_3O_2)_2 \cdot 4H_2O$ and $Fe(NO_3)_3 \cdot 9H_2O$ as the starting materials. Citric acid and ethylene glycol were used as gelling agents for the La and Mn ions in a nitrate solution. For these compositions the sol-gel fabrication process is the most adecuate due to the hugh diffusion ability of the Pb ions. This method allows shorter reaction times and lower temperatures than the ceramic one.

After drying in a sand bath at 373 K for 24 h, the gel obtained was subjected to successive heat treatments at different temperatures, 773, 973, and 1073 K, respectively, each of them for 10 h. In order to measure the electrical resistivities of the samples, the powder thus obtained was pelletized and sintered at 1173 K for 10 h in flowing oxygen.

The Mn^{3+}/Mn^{4+} content of each sample was determined by redox titration using an excess of $FeSO_4$ (0.025 M) solution and back titration with $KMnO_4$ (0.5 M). We have observed deviations from the theorical stoichiometries that could be due to an excess in the oxygen concentration or more probably to the presence of cation vacancies.[13] The iron enters in the composition of the samples as Fe^{3+}, which is the most stable oxidation state for this cation. On the other hand, the Mn^{4+} content decreases linearly (from 0.65% for the $x=0$ composition to 0.33% for the $x=0.3$ one) as the Fe doping level increases in the nominal composition of the samples. Since Fe^{3+} and Mn^{4+} have different ionic radii, 0.785 and 0.67 Å, respectively,[14] we can estimate a relative increase of about 5% in the average ionic radius between $x=0$ and 0.3 compositions. As a first consequence, the volume of the unit cell should undergo an increase as the Fe content increases, as will be discussed in a later section.

The first crystallographic characterization of the phases of samples was performed by x-ray powder diffraction analysis using a STOE equipped with a germanium monochromator, working with Cu $K\alpha_1$ radiation. At room temperature, the diffraction maxima of the La phases were indexed in a trigonal space group ($R\bar{3}c$).

Magnetic and resistance measurements were conducted in a Quantum Design MPMS-7 superconducting quantum interference device (SQUID) magnetometer. The zero-field cooling (ZFC) and field cooling (FC) curves were performed under an applied field of 10 mT. $M(T)$ curves at 1 T applied field and hysteresis loops at 10 K and up to 7 T were also obtained. The resistance and magnetoresistance versus temperature measurements were taken by a dc four-wire system with the current flowing parallel to the applied field. The pellets obtained from the synthesis procedure were cut in rectangular shape ($\approx 5\,\text{mm} \times 6\,\text{mm}$) and silver dag contacts were used. The irregularity of these contacts makes it difficult to give accurate values of the resistivity of the samples.

Electron spin resonance (ESR) spectra were recorded on a Bruker E.S.P. 300 spectrometer, equipped with a standard OXFORD low-temperature device, operating at the *X* and *Q* bands. This apparatus was calibrated by NMR probe for the magnetic field and by using a Hewlett-Packard 5352B microwave frequency counter for the resonant frequency in the cavity.

Neutron-diffraction measurements were performed at the high-flux reactor at the Institut Laue-Langevin, Grenoble, France. Three different instruments were used. For accurate refinements of the crystal and magnetic structures, measurements were carried out on D2B, using a wavelength of 1.594 Å. For tracing the temperature dependence of the structural and magnetic properties, instruments D20 and D1B were used. Using a wavelength of 2.41 Å for D20 and 2.519 Å for D1B, we studied the range $2\theta = 2° - 90°$ at temperatures ranging from 1.8 to 300 K (from 295 to 395 K for the $x=0$ sample). The Rietveld analysis of the diffraction data was performed using the FULLPROF program.[15] The line shape of the diffraction peaks was generated by a pseudo-Voigt function and the background interpolated between some fixed background points of the diagrams. The coherent neutron scattering lengths for La, Pb, Mn, Fe, and O were 8.24, 9.405, −3.73, 9.45, and 5.803 fm, respectively. In the final run the following parameters were refined: unit-cell parameters, zero-point, half-width, pseudo-Voigt, and asimmetry parameters, scale factor, atomic coordinates, and thermal isotropic factors. The occupancy factors of the La, Pb, Mn, and Fe were also allowed to vary in the last steps of the refinements. Due to the high correlation between the thermal and occupancy factors, in some cases the refinements did not reach the convergence. In these cases, the occupancy factors were fixed to the theoretical ones.

Mössbauer spectroscopy was performed in the transmission geometry using a conventional constant-acceleration spectrometer with a ^{57}Co-Rh source. Velocity was calibrated by using an Fe foil as standard material. All the spectra have been fitted using the NORMOS program.[16] Because it is not possible to study by this technique the composition $La_{0.7}Pb_{0.3}MnO_3$, another sample with 1% ^{57}Fe content was fabricated. For the $x=0.1$, 0.2, 0.3 compositions, spectra were taken at room temperature, since it happens to be in the paramagnetic region. This is not the case of the 1% ^{57}Fe content sample, which was measured at 365 K, above its Curie temperature of 330 K.

III. RESULTS

A. Magnetic properties

Some of the properties concerning the $x=0$ and 0.1 compositions were already reported by the authors in a previous work.[6] From magnetic measurements it is inferred that there is a transition from ferro- to antiferromagnetic behavior as the Fe content in the sample composition increases. Hysteresis loops measured at 10 K corroborate this trend: as can be seen in Fig. 1, samples with $x=0,0.05$ show practically the same ferromagnetic behavior. The sample with $x=0.1$ Fe doping content is still purely ferromagnetic, but the

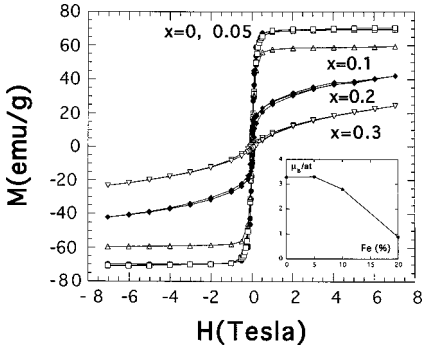

FIG. 1. Hysteresis loops measured at 10 K and up to 7 T applied field for the $La_{0.7}Pb_{0.3}Mn_{1-x}Fe_xO_3$ ($x=0.05$, 0.1, 0.2, 0.3) studied samples. The inset shows the corresponding saturation magnetic moment values.

curves obtained for $x=0.2$ and 0.3 compositions suggest a superposition of both the ferro- and antiferromagnetic components. The saturation magnetization of the ferromagnetic component has been obtained by using Arrot plots, except for the $x=0.3$ composition. The obtained values appear in the inset of Fig. 1. From the almost constant value measured for the $x=0$ and 0.05 compositions, there is a continuous decrease upon Fe doping. The substitution with Fe atoms clearly supresses the ferromagnetism. In Fig. 2, zero-field-cooled–field-cooled curves exhibit similar trends and the usual ferro- to paramagnetic transition as the temperature increases for the $x=0$, 0.05, and 0.1 compositions. The Curie temperature T_C was obtained as the minimum of the curve dM/dT calculated from measured ZFC curves. The introduction of Fe substituting the Mn ion affects strongly the measured T_C values, lowering them continuously, about 130 K for the $x=0.1$ composition. For the $x=0.2$ and 0.3 samples the magnetic behavior could be interpreted to be antiferromagnetic, showing sharp maxima in the ZFC curves (see Fig. 3). In particular, for the $x=0.2$ composition, the low-field supposed antiferromagnetic behavior together with the measured magnetic moment at high applied field clearly indicates the existence of field-induced long-range ferromagnetic order.

Using the inverse susceptibility curve and the corresponding Curie-Weiss fit $[\chi=C/(T-\theta_P)]$, we found minima in the $\chi^{-1}(T)$ behavior at 55 and 45 K for the $x=0.2$ and 0.3 corresponding compositions, respectively (see Fig. 3). These

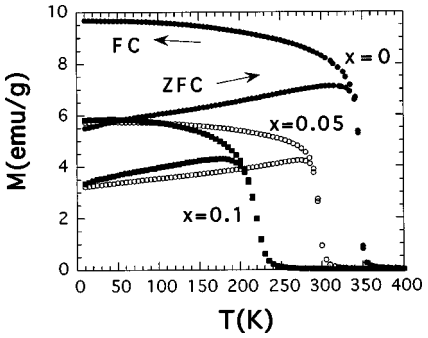

FIG. 2. Zero-field cooling (ZFC, increasing temperature arrow) and field cooling (FC, decreasing temperature arrow) magnetization vs temperature curves for the compositions corresponding to $x=0$, 0.05, and 0.1, measured at $H_{app}=10$ mT.

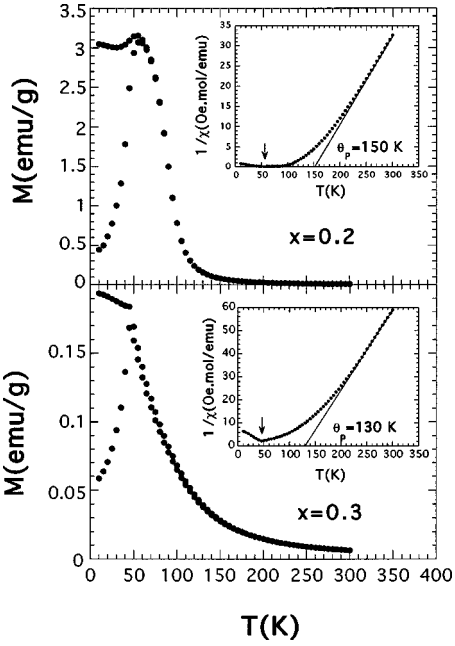

FIG. 3. Zero-field cooling and field cooling magnetization vs temperature curves for the compositions corresponding to $x=0.2$ (upper) and 0.3 (lower), measured at $H_{app}=10$ mT. The inset shows the $1/\chi$ curve obtained from zero-field cooling measurement.

temperatures could be interpreted as Néel temperatures T_N. In the high-temperature paramagnetic region, we found for the same compositions positive paramagnetic Curie temperatures $\theta_P=150$ and 130 K, respectively, which indicates the presence of strong ferromagnetic interactions still remaining in these samples. Most probably this is the case of the $x=0.2$ corresponding composition. However, it has not been possible to measure the value of any ferromagnetic component for the $x=0.3$ sample. It is clear that neutron-diffraction experiments are needed in order to elucidate the magnetic structure of these compositions. All magnetic data are summarized in Table I.

The X band ESR spectra of the samples have been recorded above and below their Curie temperature. In all cases only an averaged curve of the Mn/Fe spectra is detected. As expected, the low-temperature asymmetric signals become Lorentzian-like at $T>T_C$. A clear transition from an insulating state to a conducting one, as the temperature decreases, is observed. In Fig. 4, two recorded curves at 200 and 290 K for the composition corresponding to a 10% Fe doping level are shown. The effective g factor obtained for all composi-

TABLE I. Values of the Curie temperature T_C, magnetization per magnetic ion, $M/N\mu_B$ at 10 K and 7 T, and transition temperature in the resistance behavior, $T_{SC\text{-}M}$, for the $La_{0.7}Pb_{0.3}(Mn_{1-x}Fe_x)O_3$ ($x=0$, 0.05, 0.1, 0.2, 0.3) samples.

Sample	T_C (K)	$M/N\mu_B$	$T_{SC\text{-}M}$ (K)
$La_{0.7}Pb_{0.3}MnO_3$	345	3.28	270
$La_{0.7}Pb_{0.3}Mn_{0.95}Fe_{0.05}O_3$	295	3.3	220
$La_{0.7}Pb_{0.3}Mn_{0.9}Fe_{0.1}O_3$	215	2.79	135
$La_{0.7}Pb_{0.3}Mn_{0.8}Fe_{0.2}O_3$	$\theta_P=150$	1.98	
$La_{0.7}Pb_{0.3}Mn_{0.7}Fe_{0.3}O_3$	$\theta_P=130$	1.15	

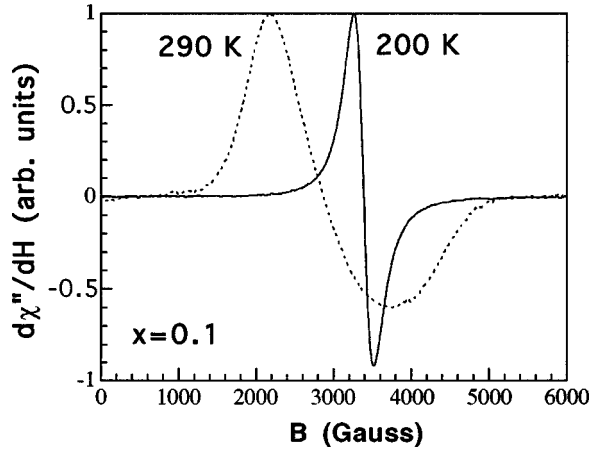

FIG. 4. X band ESR spectra for the sample $La_{0.7}Pb_{0.3}Mn_{0.9}Fe_{0.1}O_3$, measured at 290 K (insulating behavior) and 200 K (conductive behavior).

tions is ≈ 2 (at $T > T_C$). At room temperature the width of the resonance lines increases as the Fe content increases. This corresponds to a decrease of the exchange narrowing, indicating the lowering of the ferromagnetic interactions between the ions.

The dependence of the linewidth ΔH_{pp} with temperature shows minima (at 260, 150, and 140 K for the $x = 0.1$, 0.2, and 0.3 compositions, respectively) that usually are interpreted as due to spin correlation. These values correlate with the paramagnetic Curie temperature θ_P (at 250, 150, and 130 K for the $x = 0.1$, 0.2, and 0.3 compositions, respectively). This fact can be atributed either to the existence of short-range magnetic order or perhaps to the formation of ferromagnetic clusters.

B. Magnetoresistance behavior

The temperature dependence of the resistance, measured under zero applied magnetic field, for the samples with different Fe contents is shown in Fig. 5 (upper). The most remarkable fact is that only the compositions with the 5% and 10% doping amounts of Fe exhibit magnetoresistivity. Clear insulating behavior has been observed for the samples with $x = 0.2$ and 0.3, even when measuring under 6 T applied field. The relative change between 0 and 6 T applied fields on the measured resistance allows us to define its relative magnitude as $\Delta R = [R(6\,T) - R(0\,T)]/R(0\,T)$.[17] In Fig. 5 (lower), this change for the compositions corresponding to $x = 0$, 0.05, and 0.1 is shown. In these last two cases, the MR curves show a small peak ($x = 0.05$) and a shoulder ($x = 0.1$) precisely at the Curie temperature T_C. This fact clearly indicates different contributions to the magnetoresistance: an intrinsic one near the Curie temperature, due to the fact that the granular perovskite behaves in the ferromagnetic state as a granular ferromagnet and so similar to a granular transition metal.[18,19] On the other hand and especially for the sample with a 10% Fe doping level, there is a peak in the magnetoresistance at a temperature well below T_C, which does not mean a metal-insulator-like transition for the granular system, but probably reflects the difference in magnetic order between surface and core of the perovskite grains.[20]

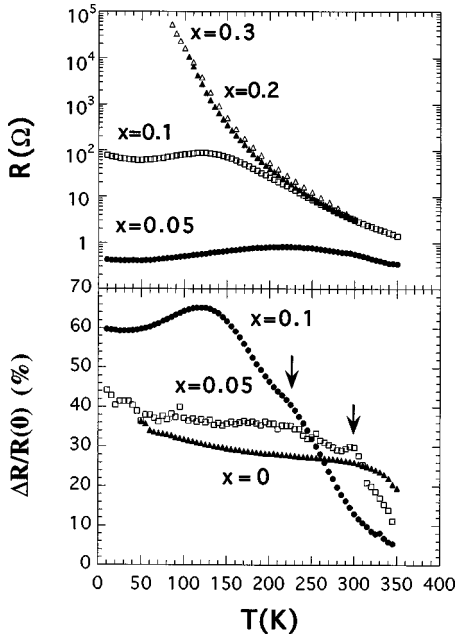

FIG. 5. Resistance vs temperature curves (upper), at 0 applied field, for the $La_{0.7}Pb_{0.3}Mn_{1-x}Fe_xO_3$ ($x = 0.05$, 0.1, 0.2, 0.3) studied samples, and magnetoresistance vs temperature curves (lower) of the $La_{0.7}Pb_{0.3}Mn_{1-x}Fe_xO_3$ ($x = 0$, 0.05, 0.1) samples, measured at 0 and 6 T applied magnetic fields.

As is clearly shown in Fig. 5 (lower), the effect of adding Fe is to increase the magnitude of the measured MR: from a value of about 30% for the noncontaining Fe sample, doping with a 10% Fe content gives rise to a 65% relative change of magnetoresistivity.

C. Neutron-diffraction study

The crystal structure of this family of compounds has been analyzed in the trigonal space group ($R\bar{3}c$), hexagonal setting ($Z = 6$), using the D2B neutron powder diffraction data obtained at room temperature. The La atoms are at (0,0,1/4) position, Mn at (0,0,0), and O at (x,0,1/4). A representation of the structure is shown in Fig. 6. For $x = 0.1$, 0.2, and 0.3, the Fe atom was placed at the Mn site, with the corresponding occupation factor for both ions. The phases with $x = 0$ and 0.1 show weak extra lines corresponding to a small amount of Mn_2O_3 as impurity ($<3\%$) (Bixbyite ASTM No. 41-1442). This impurity arises from the reduction of the Mn^{4+} cation when the solid reaction, in the presence of air, takes place. For these compositions, Mn_2O_3 was included in the refinements as second phase. Figure 7 shows the refinement of the $La_{0.7}Pb_{0.3}Mn_{0.9}Fe_{0.1}O_3$ neutron-diffraction spectrum obtained at 100 K. The final atomic parameters after the refinements are shown in Table II.

The unit-cell volume and the Mn/Fe-O distances increase with increasing Fe content. The substitution of Mn by Fe produces only a minor distortion in the MnO_6 octahedra, the O-Mn-O and Mn-O-Mn angles remaining rather constant. Furthermore, the tolerance factor (t) of the perovskite structure, $t = (d\text{La-O})/2(d\text{Mn-O})$, with dLa-O and dMn-O the La-O and Mn-O bond distances, remains constant ($t = 0.995$) for the different compositions. These geometrical characteristics indicate that the distortion of the

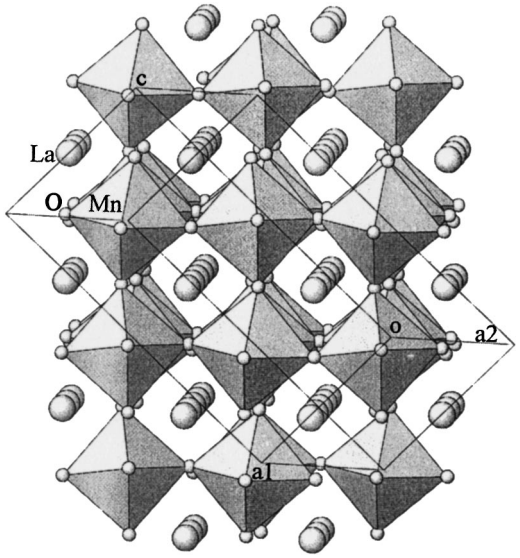

FIG. 6. A view of the $La_{0.7}Pb_{0.3}Mn_{1-x}Fe_xO_3$ crystal structure showing the relationship with the cubic perovskitelike structure. Lines represent the hexagonal unit cell. Crystallographic axes are also shown.

$La_{0.7}Pb_{0.3}Mn_{1-x}Fe_xO_3$ perovskite structure is nearly independent of the x value, in good agreement with the comparable size of Fe^{3+} and Mn^{3+} ions. The already expected volume expansion of the crystal structure arises from an increase of both the Mn/Fe-O distances and unit-cell volumes, even if this last one turns out to be lower than 1%.

The thermal evolution of the diffraction patterns for $x=0$ to 0.3 was recorded at D20 and D1B instruments. For $x=0$ and $x=0.1$, two reflections with magnetic contribution at the same d values are observed. This feature is indicative of an equivalent magnetic structure for both compounds. That is, the magnetic order does not change its structure when including a 10% of Fe in the La phases. Furthermore, all magnetic reflections can be indexed with the same cell as the nuclear one, indicating an equivalent type of ferromagnetic structure. The evolution with the temperature of the intensity peaks with magnetic contribution (012) and the overlapped (110)+(104) is shown in Fig. 8. The magnetic contribution appears at about 370 and 220 K for $x=0$ and 0.1, respectively. The Rietveld refinement of the D2B data recorded below these temperatures (270 K for $x=0$ and 100 K for $x=0.1$) was performed, taking into account the magnetic contribution as a second phase. The best solution was obtained with a collinear magnetic structure in which the magnetic moment of the Mn ion is placed into the (110) crystallographic plane, in the hexagonal setting (perpendicular to the [111] direction of the perovskite cubic cell). The obtained values of the magnetic moment are $2.44(2)\mu_B$, at $T=270\,\mathrm{K}$, for the $x=0$ composition and $2.38(2)\mu_B$, at $T=100\,\mathrm{K}$, for the $x=0.1$ one. These values are in good agreement with those obtained from magnetic measurements.

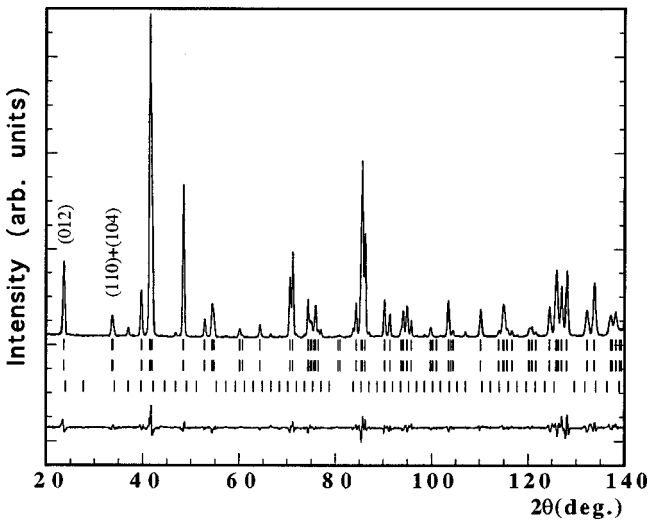

FIG. 7. Rietveld refinement of the neutron diffraction data for the sample $La_{0.7}Pb_{0.3}Mn_{0.9}Fe_{0.1}O_3$, measured at 100 K. The difference between measured and calculated data is plotted below. The second series of tick marks indicates the magnetic contribution, and the third series indicates the reflections of a minor Mn_2O_3 phase.

The thermal evolution of the diffraction patterns for $x=0.2$ and 0.3 does not show any magnetic contribution, within the experimental error, in the temperature range studied (down to 1.5 K). This lack in the long-range magnetic order and the results from magnetic measurements are in fact classic trends of a spin-glass structure in opposition to the initally supposed antiferromagnetic one. We must then talk about the spin-glass transition temperature T_{SG} of those samples, their values being $T_{SG}=55$ and 45 K for the $x=0.2$ and 0.3 compositions, respectively.

D. Mössbauer spectroscopy

The Mössbauer spectra obtained in the paramagnetic region, for all compounds, are shown in Fig. 9. The values obtained for the isommer shift ranged between IS=0.1 and 0.14 mm/s, evidence that the valence of Fe is +3. A doublet with an increase of the quadrupole splitting (QS) value, as the Fe doping level increases, is observed. This arises from the anisotropic deformation of the environment of the Fe^{3+} ions located in the distorted octahedral sites. This fact was not detected by neutron-diffraction experiments, since they give averaged magnitude values of the Mn/Fe-O distances and Mn-O-Mn bond angles. It is also the case of EPR experiments, which give only an averaged widening of the signal lines, as already discussed. In this sense, Mössbauer spectroscopy turns out to be the most appropiate technique to study the environment of the Fe atoms. In Fig. 10, the evolution of the distance d(Mn/Fe-O) and the QS value, with the Fe content, is shown. Clearly, a correlation between these two parameters exists.

IV. DISCUSSION AND CONCLUSIONS

Several authors have already reported the effect of Fe doping in colossal magnetoresistive $LaCaMnO_3$ (Refs. 21 and 22) and $LaSrMnO_3$ (Ref. 23) perovskites. In all cases the same trend is observed: as the Fe doping level in the sample increases, transition temperatures (T_C,$T_{SC\text{-}M}$) and spontaneous magnetization systematically decrease. Sample resistivity increases in a continuous way, and there is also an increase in the MR value. These changes are observed up to a 10% Fe doping level. For higher-Fe-content compositions, insulating behavior is observed in the whole temperature range studied.

TABLE II. Atomic parameters for $x=0$, 0.1, 0.2, and 0.3 after the Rietveld refinements of the D2B neutron-powder-diffraction data at room temperature. Space group ($R\bar{3}c$), $Z=6$. La and Pb atoms are at $6a$ positions (0, 0, 1/4); Mn and Fe atoms are at $6b$(0,0,0); O atoms are at $18e(x,0,1/4)$.

Sample	$x=0$	$x=0.1$	$x=0.2$	$x=0.3$
T (K)	270	270	300	300
a (Å)	5.5167(1)	5.5235(1)	5.5272(1)	5.5302(1)
c (Å)	13.3954(1)	13.3978(1)	13.4115(2)	13.4146(2)
V (Å)	353.05(1)	353.99(1)	354.83(1)	355.29(1)
t	0.995	0.994	0.995	0.994
La B(Å^2)/F_{OCC}	0.52(2)/0.756	0.57(3)/0.756	0.85(2)/0.7	0.86(2)/0.7
Pb B(Å^2)/F_{OCC}	0.52(2)/0.246	0.57(3)/0.246	0.85(2)/0.3	0.86(2)/0.3
Mn B(Å^2)/F_{OCC}	0.39(3)/1.0	0.79(8)/0.924(1)	0.85(2)/0.8	0.86(2)/0.7
Fe B(Å^2)/F_{OCC}		0.79(8)/0.096(1)	0.85(2)/0.2	0.86(2)/0.3
O x	0.4592(1)	0.4569(1)	0.4574(1)	0.4567(1)
O B(Å^2)/F_{OCC}	0.95(1)/3.0	1.11(2)/3.0	1.33(1)/3.0	1.26(2)/3.0
Mn/Fe-O (Å)	1.9578(4)×6	1.9610(4)×6	1.9622(4)×6	1.9636(4)×6
La/Pb-O (Å)	2.5333(7)×3	2.5236(5)×3	2.5283(7)×3	2.5256(8)×3
	2.7516(2)×6	2.7541(2)×6	2.7564(3)×6	2.7576(4)×6
	2.9834(7)×3	3.0000(5)×3	2.9989(7)×7	3.0045(6)×3
⟨La/Pb-O⟩ (Å)	2.755	2.758	2.760	2.7613
Mn/Fe-O-Mn/Fe (deg)	166.80(4)	166.06(4)	166.23(4)	165.99(4)
O-Mn/Fe-O (deg)	90.71(2)	90.79(2)	90.77(2)	90.79(2)
Mn_2O_3 (%)	2.73	2.57		
Discrepancy factors				
R_p (%)	4.71	4.82	4.20	4.74
R_{wp} (%)	6.69	6.13	5.32	5.97
R_e (%)	1.90	3.09	3.91	3.63
χ^2	1.25	3.92	1.85	2.7
R_B (%)	3.72	3.89	3.93	5.53
R_M (%)	6.47	6.50 (100 K)		

It has been already well established that the double-exchange mechanism mediates ferromagnetism and metallic conduction. However, our experimental work evidences that the partial replacement of Mn by Fe atoms favors insulating and antiferromagnetic behavior, in opposition to the effects of the double exchange. Taking into account that Mn^{3+} and Fe^{3+} have very similar ionic sizes in octahedral high-spin coordination, the influence in the lattice parameters can be neglected as it has been proved by neutron-diffraction experiments. So the mechanism that suppress the double exchange must arise only from the electronic structure of the atoms.

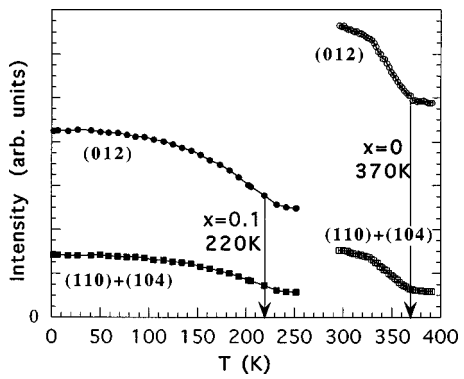

FIG. 8. Temperature dependence of the intensity of the Bragg peaks (012) and the overlapped (110)+(104), for the $x=0$ and 0.1 compositions. Lines are a guide for the eyes.

The experimental results obtained for our samples are in agreement with previous studies concerning the transport properties of the $LaBaMnFeO_3$ family of compounds.[20,24] Those studies demonstrated that for similar doping Fe levels than those reported in this work, Fe^{3+}, Mn^{3+}, and Mn^{4+} ions are present. The $t_{2g\uparrow}$ levels are fully occupied, the $t_{2g\downarrow}$ and $e_{g\downarrow}$ levels are empty, and the energies of the $e_{g\uparrow}$ ones will determine the electron distribution of the Fe and Mn atoms. Following the nominal stoichiometry of our samples, the Fe $e_{g\uparrow}$ level is fully occupied and $[(0.7-x)/2(1-x)]$ of the Mn $e_{g\uparrow}$ level is also filled, considering the latter factor one-half of the fraction of Mn^{3+} ions. This will give us the position of the Fermi surface above the top of the Fe $e_{g\uparrow}$ level, assuming uniformity in the filling for simplicity. With the values $x=0$, 0.1, 0.2, and 0.3, of our compositions, the Fermi surface will lie between 0.28 and 0.35 eV above the top of that band (see Fig. 11). The width of the $e_{g\uparrow}$ level has been stimated to be around 1 eV.[25] It is clear that electron hopping between Fe and Mn is not possible due to the lack of available states in the Fe $e_{g\uparrow}$ level. The only vacant states will locate in the Fe $t_{2g\downarrow}$ one. However, it has been demonstrated that the Fe $t_{2g\downarrow}$ lies around 2 eV above the top of the Fe $e_{g\uparrow}$ level,[26]

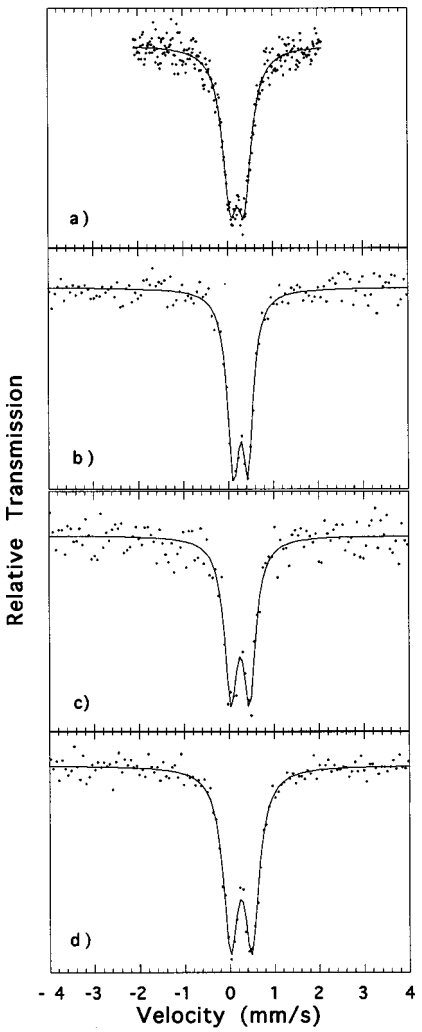

FIG. 9. Fitted Mössbauer data collected for the $La_{0.7}Pb_{0.3}Mn_{1-x}Fe_xO_3$ system in the paramagnetic region: (a) $x=0.01$ (at $T=365$ K), (b) $x=0.1$, (c) $x=0.2$, and (d) $x=0.3$ (at room temperature).

and so about 1.65–1.72 eV above the Fermi level of our system. As a direct consequence, the electron hopping from Mn to Fe is energetically forbidden, and only the Mn $e_{g\uparrow}$ band is electronically active, electronic hopping occurring still between Mn^{3+} and Mn^{4+}. On the other hand and from electrical resistance measurements, we have calculated a

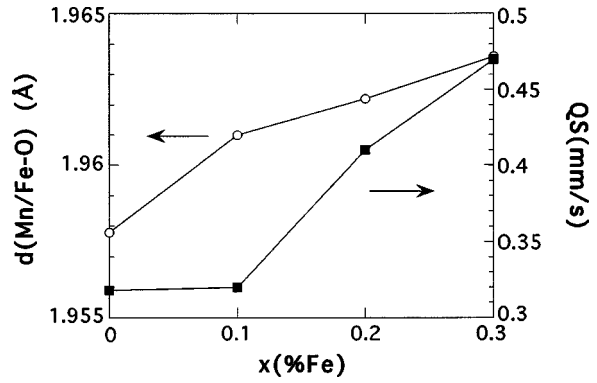

FIG. 10. Dependence of the distance d(Mn/Fe-O) and the quadrupole splitting (QS) with the Fe content, for the studied samples.

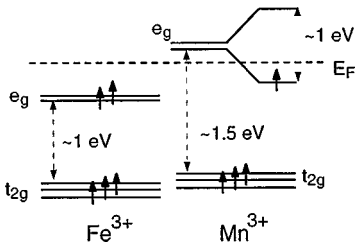

FIG. 11. Energies level diagram of Fe and Mn in $La_{0.7}Pb_{0.3}Mn_{1-x}Fe_xO_3$ samples.

value of the forbidden energy gap around 0.2–0.3 eV (see Fig. 12) for the samples corresponding to $x=0.2$ and 0.3. These obtained low values could explain the appearance of ferromagnetic interactions (thermically activated electron level hopping) around room temperature, which should explain the high paramagnetic Curie temperatures obtained for those compositions.

From our measurements it is clear that the Fe enters in these compositions as Fe^{3+}, giving rise to an antiferromagnetic coupling between Mn and Fe ions that favors the superexchange mechanism. However, if titration data about Mn^{4+} content are reliable, the Mn^{3+}/Mn^{4+} ratio increases with the Fe content. The Fe^{3+} will fix also the nearest-neighbor spins, reducing mainly the population of hopping electrons and available hopping sites. Double exchange is then progressively suppressed, weakening the ferromagnetism and metallic behavior of the samples.

In conclusion, the ferromagnetic character of the samples studied in this work remains unchanged up to a 10% Fe doping level. Nevertheless, a progressive decrease of the Curie temperature values and saturation magnetic moment is observed. These compositions show magnetoresistive behavior, being a 65% relative change measured for the $x=0.1$ composition.

For the samples corresponding to $x=0.2$ and 0.3, neutron-diffraction experiments revealed that there is no magnetic contribution in the 1.5–300 K temperature range. In the case of the sample with a 20% Fe doping level, from low-field magnetic measurements and especially from the extrapolated (Arrot plot) value of the magnetic moment at high applied field values ($\mu_0 H>2$ T), we can infer that this composition shows a three-dimensional long-range field-induced ferromagnetic order. Finally, the $x=0.3$ corresponding composi-

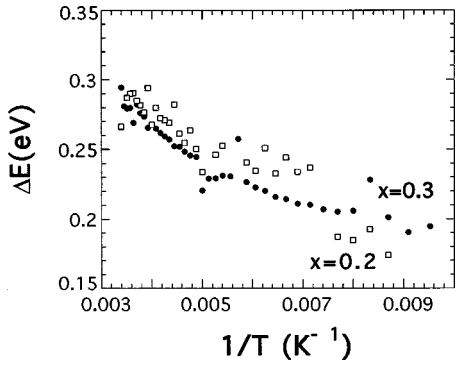

FIG. 12. Forbidden energy gap vs $1/T$, for the $x=0.2$ (open symbols) and 0.3 (solid symbols) studied samples.

tion shows clear features of a spin-glass system. The presence of ferromagnetic clusters in these samples could explain the high θ_P measured values and linewidth broadening observed in the EPR measurements at the same temperatures. Both $x=0.2$ and 0.3 samples show clearly insulating behavior.

ACKNOWLEDGMENTS

This work was financially supported by the Basque Government under Project No. PGV 96/94. We wish to thank Dr. J. Garitaonaindia for helpful discussions about Mössbauer spectroscopy.

[1] G. H. Jonker and J. H. van Santen, Physica (Amsterdam) **16**, 337 (1950).
[2] H. Y. Hwang, S.-W. Cheong, P. G. Radaelli, M. Marezio, and B. Batlogg, Phys. Rev. Lett. **75**, 914 (1995).
[3] P. Schiffer, A. P. Ramírez, W. Bao, and S.-W. Cheong, Phys. Rev. Lett. **75**, 3336 (1995).
[4] A. Maignan, F. Damay, C. Martin, and B. Raveau, Mater. Res. Bull. **32**, 965 (1997).
[5] L. Righi, P. Gorria, M. Insausti, J. Gutiérrez, and J. M. Barandiarán, J. Appl. Phys. **81**, 5767 (1997).
[6] J. Gutiérrez, J. M. Barandiarán, M. Insausti, L. Lezama, A. Peña, J. J. Blanco, and T. Rojo, J. Appl. Phys. **83**, 7171 (1998).
[7] C. Zener, Phys. Rev. **82**, 403 (1951).
[8] M. Pissas, G. Kallias, E. Devlin, A. Simopoulos, and D. Niarchos, J. Appl. Phys. **81**, 5770 (1997).
[9] T. Venkatesan, M. Rajeswari, Z. Dong, S. Ogale, and R. Ramesh, Philos. Trans. R. Soc. London, Ser. A **356**, 1661 (1998).
[10] C. W. Searle and S. T. Wang, Can. J. Phys. **48**, 2023 (1970).
[11] A. V. Powell, C. Herwing, D. C. Colgan, and A. G. Whittaker, J. Mater. Chem. **8**, 119 (1998).
[12] C. J. Brinker and G. R. Scherer, *Sol-Gel Science: The Physics and Chemistry of Sol-Gel Processing* (Academic, New York, 1990).
[13] C. N. R. Rao, A. K. Cheetham, and R. Mahesh, Chem. Mater. **8**, 2421 (1996).
[14] R. D. Shannon, Acta Crystallogr., Sect. A: Cryst. Phys., Diffr., Theor. Gen. Crystallogr. **32**, 751 (1976).
[15] J. Rodríguez-Carvajal, computer code FULLPROF, Rietveld Pattern Matching Analysis of Powder Patterns, ILL, Grenoble, 1990.
[16] R. A. Brand, J. Lauer, and D. M. Harlach, J. Phys. F: Met. Phys. **14**, 555 (1984).
[17] K. Chahara, T. Ohno, M. Kasai, and Y. Kozono, Appl. Phys. Lett. **63**, 1990 (1993).
[18] S. Jin, Science **264**, 413 (1994).
[19] R. von Helmollt, Phys. Lett. **54A**, 225 (1975).
[20] N. Zhang, W. Ding, W. Zhong, D. Xing, and Y. Du, Phys. Rev. B **56**, 8138 (1997).
[21] E. Banks and N. Tashima, J. Appl. Phys. **41**, 1186 (1970).
[22] K. H. Ahn, X. W. Wu, K. Liu, and C. L. Chien, Phys. Rev. B **54**, 15 299 (1996).
[23] A. Ajan, N. Venkataramani, S. Prasad, S. N. Shringi, A. K. Nigam, and R. Pinto, J. Appl. Phys. **83**, 7169 (1998).
[24] G. H. Jonker, Physica (Amsterdam) **20**, 1118 (1954).
[25] J. M. D. Coey, M. Viret, L. Ranno, and K. Ounadjela, Phys. Rev. Lett. **75**, 3910 (1995).
[26] A. Chainani, M. Mathew, and D. D. Sarma, Phys. Rev. B **48**, 14 818 (1993).